PHYSICAL REVIEW B VOLUME 51, NUMBER 8 15 FEBRUARY 1995-II

Electronic structure of graphite: Effect of hydrostatic pressure

R. Ahuja
Condensed Matter Theory Group, Department of Physics, Uppsala University, Box 530, S-751 21, Uppsala, Sweden

S. Auluck
Department of Physics, University of Roorkee, Roorkee-247 667, India

J. Trygg
Condensed Matter Theory Group, Department of Physics, Uppsala University, Box 530, S-751 21, Uppsala, Sweden

J. M. Wills
Center for Materials Science and Theoretical Division, Los Alamos National Laboratory, Los Alamos, New Mexico 87544

O. Eriksson and B. Johansson
Condensed Matter Theory Group, Department of Physics, Uppsala University, Box 530, S-751 21, Uppsala, Sweden
(Received 31 August 1994)

We present theoretical results for the electronic structure of graphite using a full potential linear muffin-tin orbital method. The calculations are performed at ambient pressure and at hydrostatic pressures of 5 and 10 GPa. Our ambient pressure results are in agreement with recent independent calculations as well as with experimental photoemission data. Our calculations at 5 and 10 GPa show a splitting of the σ bands indicating an increase in the overlap between wave functions centered on different carbon atoms. The calculated pressure dependence of the A_1 and A_2 transitions (attributed to transitions occurring at the symmetry point K) is in agreement with recent optical reflectivity data. Also, the compressibility is calculated to be highly anisotropic, in excellent agreement with experimental data.

I. INTRODUCTION

Graphite can be regarded as a prototype of layered crystals. It is known to have many technological applications and as a result graphite has been studied vigorously both theoretically and experimentally for the past few decades. Hexagonal graphite has an abnormally large c/a ratio (c/a=2.7259). This gives rise to a large anisotropy in its structural and electronic properties. The carbon atoms in the basal plane are bound together by strong covalent bonds (σ) while the atoms in the adjacent planes are weakly bound by Van der Waal bonds. Thus the interlayer nearest neighbor distance (3.35 Å) is much larger than the in-plane nearest neighbor distance (1.42 Å). The bonding properties of graphite can be explained by so-called sp^2 hybrids. Three of the four valence electrons are assigned to the trigonally directed sp^2 hybrids forming (σ) bonds while the fourth electron lies in the p_z orbital normal to the σ bonding plane, forming weak π bonds. The weak interaction between layers introduces small splittings for the π and π^* bands.

There exist a number of measurements of the structural and electronic properties of hexagonal graphite. The physical properties of graphite have been extensively studied through Raman scattering,[1–4] infrared reflectance,[2,5–7] inelastic neutron scattering,[8] elastic constant measurements,[9] angle-resolved photoemission,[10–13] and inverse photoemission[13–18] experiments. It has been established that in general the results of various experiments are in agreement with energy-band calculations at ambient pressure (see below). However, under pressure, there seems to have been much less work done as regards comparison between theory and experiment for graphite. Our purpose of this work is to provide an electronic structure calculation for graphite under hydrostatic pressure and compare it with experimental data. We will also calculate the compressibility of graphite, and specifically address the pronounced anisotropy.

The band structure of graphite close to the Fermi energy (E_F) was first calculated by McClure[19] and Slonczewski and Weins[20] (commonly known as the SWMcC model) using the $\mathbf{k}\cdot\mathbf{p}$ method. In this model the energy eigenvalues near E_F are given in terms of seven parameters which define the interaction energies between the orbitals from different carbon atoms within the basal plane and carbon atoms in the neighboring planes. As this model is very usable, it has been popular to use experimental data and fit the different parameters so that theory and experiment agree. In this context it is encouraging that there is agreement between the values of the parameters obtained from the de Haas–van Alphen (dHvA) and optical experiments.[21,22] The model can also be used to interpret the experimental data obtained under high pressure.[6]

The electronic structure of graphite has also been calculated self-consistently by means of the local den-

sity approximation (LDA) by numerous workers using different computational methods such as the linear combination of atomic orbitals method (LCAO),[23] the Korringa-Kohn-Rostoker (KKR) method,[24] the full-potential linearized augmented plane wave (FPLAPW) method,[25,26] the pseudopotential (PP) method,[27–29] and the linear muffin-tin-orbitals (LMTO)[30] method within the atomic sphere approximation (ASA). The band structures obtained by the different methods are in general agreement with each other and with photoemission experiments.[27,29] However, there is a discrepancy with respect to the position of the top of the σ band relative to E_F. Pseudopotential calculations[27–29] put this around 3.0 eV below E_F, while the FPLAPW calculations[25,26] put it around 4–6 eV below E_F. Experimentally it is observed at 4.6–5.5 eV below E_F and the agreement between theory and experiment is fair.

Although there exist *ab initio* band calculations for hexagonal graphite at ambient pressure, there is considerably less theoretical work on compressed graphite. As a matter of fact, only one calculation on compressed graphite has been performed[30] using a somewhat less accurate method. Such calculations are of interest since under pressure the c axis becomes much more compressed than the a axis. In fact the linear compressibility parallel to the c axis is 35 times larger than that perpendicular to it.[4] Thus the interlayer distance between the carbon atoms decreases rapidly whereas the intralayer distances remain almost constant. With increasing pressure one should therefore see a gradual change from a quasi-two-dimensional behavior to a three-dimensional behavior. Moreover, optical data exist for graphite under pressure and we will compare our calculations with these data. The calculation in Ref. 30 yielded eigenvalues near the symmetry point K which were in agreement with experiment but gave the bottom of the σ band around 16 eV below E_F, which is 4 eV less than the experimental value. This could be attributed to the accuracy of the calculational method and to the many (14) empty spheres introduced in the calculation.

In the present paper we report on electronic structure calculations of graphite at ambient pressure and under compression, using a method which does not rely on approximations concerning the geometry of the calculated potential and which is based on the so-called linear muffin-tin-orbital method (see below), i.e., the FPLMTO.

II. DETAILS OF CALCULATIONS

In our present calculations we used a full-potential linear muffin-tin-orbital (FPLMTO) technique.[31] The calculations were all electron. The charge density and potential were allowed to have any shape inside the muffin tins as well as in the interstitial region. The basis set, charge density, and potential were expanded in spherical harmonic series (with a cutoff $l_{\max}=8$) within the nonoverlapping muffin-tin spheres and in a Fourier series in the interstitial region. The basis set was comprised of augmented linear muffin-tin-orbitals.[32,33] The tails of the basis function outside their parent spheres were linear combinations of Hankel or Neuman functions with nonzero kinetic energy. The integration over the Brillouin zone was done using the special point sampling[34] with a Gaussian smearing of 20 mRy and using 108 k points in $\frac{1}{12}$th of the Brillouin zone. The calculations were done at the experimental lattice constants. The potential was calculated using the local density approximation with the Hedin-Lundqvist[35](HL) expression for the exchange and correlation potential.

III. ELECTRONIC STRUCTURE RESULTS

A. At ambient pressure

We have calculated the electronic structure of graphite at ambient conditions and at experimental volumes corresponding to pressures of 5 and 10 GPa. The lattice constants corresponding to these three pressures are taken from the work of Hanfland *et al.*[4] and are given in Table I. We first consider the ambient pressure results. The energy-band structure at this volume is plotted in Fig. 1. We find that the band structure in Fig. 1 agrees well with the other calculations.[28,29] To illustrate this we show in Table II the energy eigenvalues at the symmetry point Γ and compare them with some recent calculations and also with values deduced from photoemission experiments. Note that there is good agreement between all the theoretical calculations and experiment. For the bottom of the σ and π bands the different calculations agree with experiment to within 1 eV. For the top of the σ band the LAPW[25,26] and the KKR[24] results are in better agreement with the experimental data compared to the result of the present investigation as well as with the PP[28,29] and LCAO[23] results which give 1.0–1.5 eV lower values. For the unoccupied σ^* bands we have taken the mean value of the three levels for the different calculations and compared it with the experimental data; the agreement is within 1 eV. Such a difference between experiment and theory is not uncommon in the LDA.[36] Differences between the various theoretical calculations might be attributed to differences in the exchange-correlation poten-

TABLE I. Lattice parameters and the experimental pressure for graphite as a function of volume. Experimental values are from Ref. 4.

Volume (Å^3)	Experimental pressure (GPa)	Experimental c/a	Calculated c/a
8.80	0.0	2.72	2.77
8.44		2.63	2.63
8.25		2.58	2.57
8.01	5.0	2.51	2.48
7.77		2.46	2.43
7.61	10.0	2.42	2.39
7.42	13.0	2.38	2.34
7.04			2.25
6.60			2.15
6.16			2.05

TABLE II. Characteristic energy levels (in eV) for graphite relative to the Fermi energy.

	Present work	Other theoretical calculations				Experimental
Bottom σ	-19.2	-19.4[a]	-20.1[b]	-19.6[c]	-20.8[d]	-19.5[e]	-20.6[f]
			-19.8[b]	-19.3[c]	-20.5[d]	-19.2[e]	
Bottom π	-7.8	-7.7[a]	-8.9[b]	-8.7[c]	-9.1[d]	-8.2[e]	-8.1,[f]-8.5[g]
	-6.4	-6.6[a]	-6.8[b]	-6.7[c]	-7.1[d]	-6.5[e]	-7.2,[f]-5.7,[h]-6.6[g]
Top σ	-3.4	-3.0[a]	-3.5[b]	-4.6[c]	-3.4[d]	-4.3[e]	-4.6,[f]-5.5[g]
			-3.4[b]	-4.6[c]	-3.3[d]	-4.3[e]	
Unoccupied σ^*	5.7	4.0[a]	3.7[b]	3.8[c]	3.7[d]	7.1[e]	
	7.9	8.2[a]	7.9[b]	8.3[c]	9.0[d]	7.3[e]	6.9[f]
	8.0		7.9[b]	8.4[c]	9.3[d]	7.3[e]	
π bands at point K							
ε_1^0 - ε_3^0	0.57		0.80[b]		0.7[d]	0.44[e]	0.72,[i]0.68[j]
ε_3^0 - ε_2^0	0.68		0.86[b]		0.8[d]	0.61[e]	0.84,[i]0.81[j]

[a] Schabel and Martins (Ref. 29).
[b] Charlier *et al.* (Ref. 28).
[c] Jansen and Freeman (Ref. 25).
[d] Holzwarth *et al.* (Ref. 27).
[e] Tatar and S.Rabii (Ref. 24).
[f] Eberhardt *et al.* (Ref. 11).
[g] Law *et al.* (Ref. 12).
[h] Bianconi *et al.* (Ref. 38).
[i] Bellodi *et al.* (Ref. 7).
[j] Hanfland *et al.* (Ref. 6).

tials or to differences in the number of **k** points used for obtaining a self-consistent potential. It might also be due to differences in the methods used. A far more stringent test of the calculated electronic structure is provided by the eigenvalues at the symmetry point K. These are also given in Table II. Once again there is good agreement between the present as well as with the previous calculations and experiment, with deviations in the range of 0.2 eV. It is interesting to calculate the SWMcC model parameters using our present energy-band structure. We have not made an attempt to determine all the parameters but using the eigenvalues at the symmetry point K we obtain $\gamma_2 = -0.012$ eV, $\gamma_1 = 0.315$ eV, and $\Delta+\gamma_5 = 0.043$ eV. Using the eigenvalues at the symmetry point H we obtain that $\gamma_6 \simeq -0.022$ eV. These values are in agreement with the current accepted values.[28]

The density of states (DOS) is shown in Fig 2. Notice that the DOS is characterized by a very low value at the Fermi level E_F. The occupied part of the DOS is composed of an s component and a p component, with the s component dominating at lower energies and the p component being more pronounced at higher energies. This is connected to the fact that the s orbitals participate in building up the sp^2 hybrids which then form the low lying σ bands in Fig. 1. The higher lying π bands have p_z character only. Our calculations yield a DOS at the Fermi energy $D(E_F) = 0.09$ states/Ry cell to be compared with the experimental value of 0.145 states/Ry cell derived from heat capacity measurements.[37] It should be noted here that the theoretical DOS at E_F does not include exchange or phonon enhancements, which are present in the experiment. The low value of the DOS at E_F is also well documented using X-Ray photoemission spectroscopy.[38]

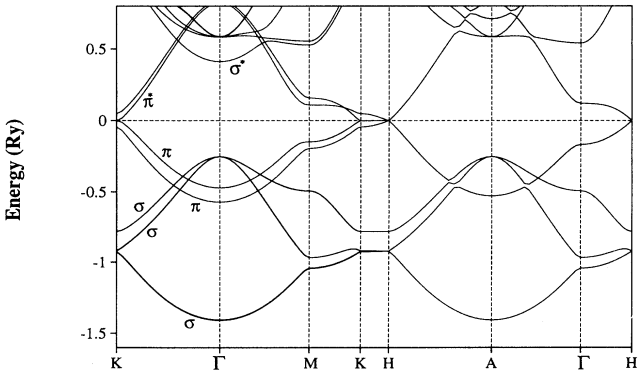

FIG. 1. Energy bands of graphite at the equilibrium volume along the major symmetry directions. The Fermi level (E_F) is set at zero energy.

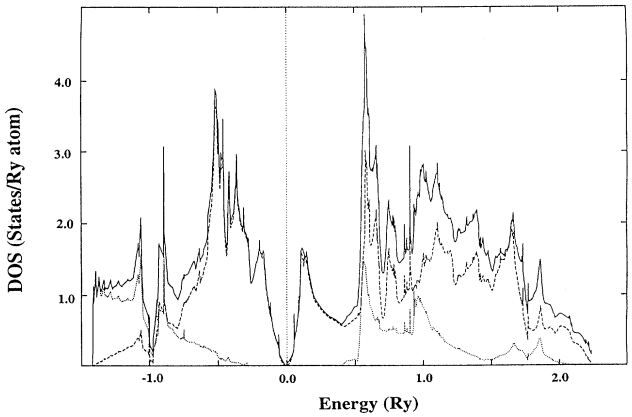

FIG. 2. Calculated density of states (DOS) for graphite. The full line shows the total DOS, while the dotted and dashed lines show the s partial and p partial DOS's, respectively. The Fermi level is set at zero energy and marked by a vertical dotted line.

B. Compressed graphite

The band structures calculated with the experimental lattice parameters corresponding to 5 and 10 GPa are plotted in Figs. 3(a) and 3(b). If we now compare the energy bands obtained at the three different volumes [Figs. 1, 3(a), and 3(b)] we observe first of all that in the K-H direction the bands show little dispersion. This is a reflection of the fact that the system is quasi-two-dimensional and that the atomic layers along the z axis have very little wave-function overlap, since the K-H direction corresponds to changing only the z coordinate of the **k** vector. However, note that with increasing pressure the dispersion in the K-H direction becomes more pronounced. This is especially true for the π bands; the σ bands in the K-H direction are affected only very little by the increased pressure. This is also easily understood since with pressure it is mainly the interatomic distance in the z direction which is reduced. The overlap between the p_z orbitals should therefore increase causing a larger change in the width of the π bands, whereas the sp^2 orbitals (which are lying in the xy plane) are not modified by a decreased intralayer splitting. Thus at 10 GPa graphite is showing signs of transforming from a two- to a three-dimensional system. Also, the degeneracy at the bottom of the σ band is another manifestation of the two-dimensional character of the electronic structure. When we compare the zero pressure band structure with those of Figs. 3(a) and 3(b) we notice that the degeneracy of the bottom of the σ band is lifted and this splitting increases with pressure. Also some minor splittings are seen in the other σ bands for compressed graphite.

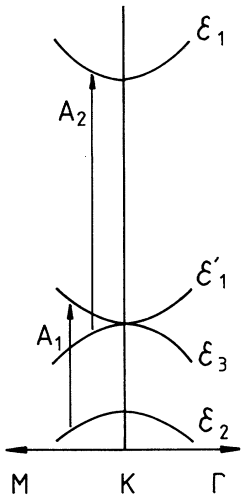

FIG. 4. Schematic energy-band structure of graphite near the edge of the Brillouin zone. The arrows show the A_1 and A_2 interband transitions.

Hanfland *et al.*[6] have measured the optical reflectivity of graphite up to pressures of 12 GPa. From an analysis of their data they have identified the structure in the reflectivity as originating from the A_1 and A_2 tran-

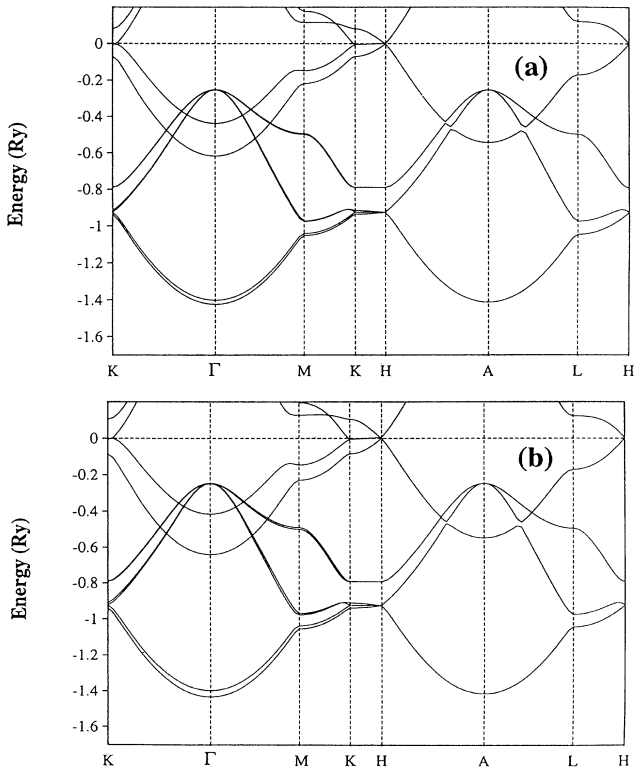

FIG. 3. Energy bands of graphite along the major symmetry directions (a) at 5 GPa and (b) at 10 GPa. The Fermi level (E_F) is set at zero energy.

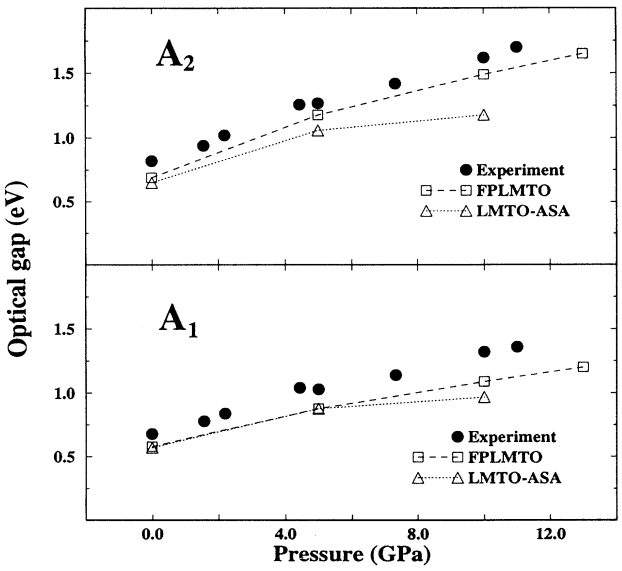

FIG. 5. Pressure dependence of the A_1 and A_2 interband transitions. The filled circles correspond to the experimental data of Hanfland *et al.* (Ref. 6). The theoretical data obtained from the present calculations and the data calculated by Auluck and Brooks (Ref. 30) are shown by open squares and triangles, respectively.

TABLE III. Pressure dependence of optical transitions at point K.

Pressure (GPa)	Method	A_1 (eV)	A_2 (eV)	$A_1 - A_2$ (eV)
0	Experiment[a]	0.68	0.82	0.14
	LMTO-ASA[b]	0.57	0.65	0.08
	FPLMTO	0.58	0.69	0.11
5	Experiment[a]	1.03	1.27	0.24
	LMTO-ASA[b]	0.88	1.06	0.18
	FPLMTO	0.88	1.18	0.30
10	Experiment[a]	1.32	1.62	0.30
	LMTO-ASA[b]	0.97	1.18	0.21
	FPLMTO	1.09	1.49	0.40

[a]Hanfland *et al.* (Ref. 6).
[b]Auluck and Brooks (Ref. 30).

sitions occurring at the symmetry point K. These transitions are illustrated in Fig. 4, where we have plotted a schematic band structure near K. As a function of pressure the band structure changes and hence it is expected that the A_1 and A_2 transitions change. From our calculated electronic structure we directly obtain values for these transitions as a function of pressure from the eigenvalues at the symmetry point K (see Figs. 1 and 3). In Table III we list our calculated transition energies together with experimental data and find that the agreement is good. We note that the LMTO-ASA calculation,[30] which did not give a good agreement for the energy eigenvalue at the Γ point, also gives a good agreement with the experimental pressure dependence of the transitions. The calculated pressure dependence of the A_1 and A_2 transitions is shown in Fig. 5 along with experimental data. We see that although the LMTO-ASA calculations give the correct pressure dependence of the A_1 and A_2 transitions, the FPLMTO calculation shows a marked improvement over the LMTO-ASA results.[30] We have also calculated the logarithmic pressure derivatives of the A_1 and A_2 transitions, and these are given in Table IV.

IV. STRUCTURAL RESULTS

We have calculated the c/a ratio of graphite as a function of volume. That is to say, for each volume we have minimized the total energy with respect to the crystallographic c/a parameter. The result of this calculation is displayed in Fig. 6 and in Table I, together with experimental data. Notice that the agreement between experiment and theory is very good and that the calculations slightly overestimate the compressibility in the z direction. At the experimental volume the c/a ratio is ~2.7. However, at the lowest studied volume in Fig. 6 this ratio is reduced to ~ 2.1. Hence, even at a volume of 6.16 Å^3/atom graphite is best described as being quasi-two-dimensional, but for very high pressures it is rapidly transforming to a more isotropic material, as shown in Fig. 6. To illustrate this further we display the charge density contour of graphite. First we show the charge density contour for graphite at ambient pressure for a cut in the xy plane (Fig. 7). The hexagonal graphite layers are in the xy-plane and from Fig. 7 we see the hexagonal arrangement of the atoms with covalent bonds between the different atoms with a characteristic *butterfly* electron density distribution. The directionality of the sp^2 hybrids can thus be seen immediately from this figure. The charge density contour in this plane looks quite similar for compressed graphite and therefore we do not show it. In Fig. 8 we show the charge density in the yz plane for two volumes, 8.80 Å^3/atom [Fig. 8(a)] and 7.61 Å^3/atom [Fig. 8(b)]. The quasi-two-dimensional behavior of graphite is obvious from the charge density distribution in the yz plane, since most of the charge is found within the plane, with very little overlap between the different planes. However, the overlap and interaction between the different planes is increasing substantially with pressure, as is obvious when comparing Figs. 8(a) and 8(b). The charge density in Fig. 8(b) is extended more in the region between the planes.

TABLE IV. Logarithmic pressure derivative of A_1 and A_2 (see text).

	Experiment[a] (GPa^{-1})	LMTO-ASA[b] (GPa^{-1})	FPLMTO (GPa^{-1})
$\frac{d \ln A_1}{dp}$	0.127(7)	0.109	0.103
$\frac{d \ln A_2}{dp}$	0.129(7)	0.126	0.142

[a]Hanfland *et al.* (Ref. 6).
[b]Auluck and Brooks (Ref. 30).

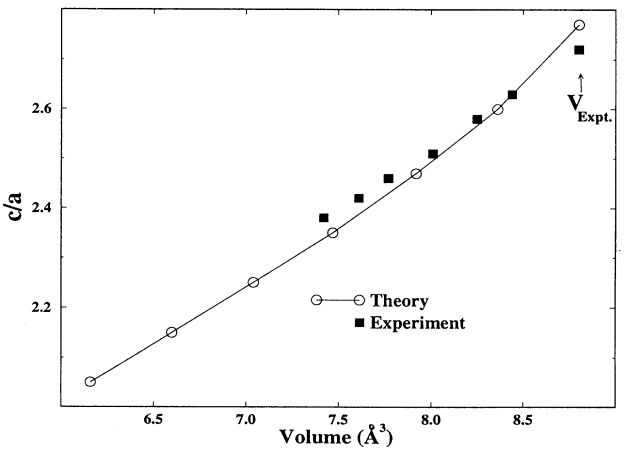

FIG. 6. The variation of the axial ratio c/a of hexagonal graphite as a function of volume. The present theoretical data are shown by open circles and the filled squares correspond to the experimental data of Hanfland *et al.* (Ref. 4).

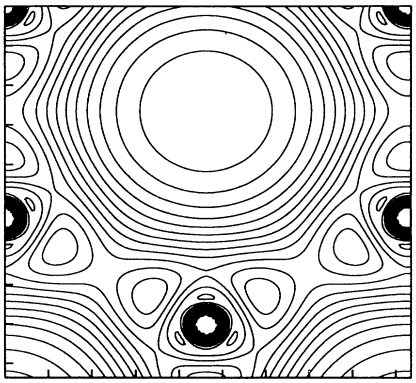

FIG. 7. Charge-density contours for hexagonal graphite at the experimental equilibrium volume (8.80 Å^3/atom). The contours are shown for a cut in the xy plane.

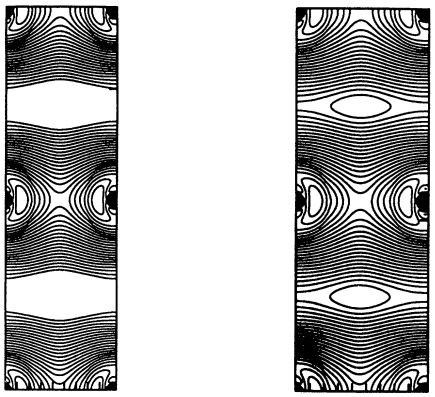

FIG. 8. Charge-density contours for hexagonal graphite at a volume of 8.80 Å^3/atom (a) and 7.61 Å^3/atom (b). The contours are shown for a cut in the yz plane.

V. CONCLUSIONS

To conclude, we have calculated the band structure of graphite using the FPLMTO method and have found good agreement with the photoemission data as well as with other *ab initio* calculations based on the LCAO, KKR, PP, and LAPW methods. The reflectivity data can be explained from transitions occurring at the symmetry point K. Our calculated values for the optical transitions are in good agreement with experimental data. We have also calculated the band structure of graphite corresponding to hydrostatic pressures of 5 and 10 GPa. Our calculations show splittings of the σ bands when the volume is reduced and this is associated with an increase in the interaction between the carbon atoms lying in neighboring planes due to the decrease in the lattice constant c. The pressure dependence of the optical transitions (near K) are in agreement with the experimental data. Finally, the calculated c/a ratio is decreasing rapidly with increasing pressure, in excellent agreement with experiment.

ACKNOWLEDGMENTS

B.J. and O.E. wish to thank the Swedish Natural Science Research Council for financial support. S.A. would like to thank the Condensed Matter Theory Group at Uppsala University for their kind hospitality. Part of these calculations were done at the Swedish Supercomputer Centre in Linköping, Sweden.

[1] F. Tuinstra and J.L. Koenig, J. Chem. Phys. **53**, 1126 (1970).
[2] L.J. Brillson, E. Burstein, A.A. Maradudin, and T. Stark, in *Physics of Semimetals and Narrow Gap Semiconductors*, edited by D.L. Carter and R.T. Bate (Pergamon, New York, 1971), p. 187.
[3] R.J. Nemanich, G. Lucovsky, and S.A. Solin, in *Proceedings of the International Conference on Lattice Dynamics*, edited by M. Balkanski (Flammarion, Paris, 1975), p. 619.
[4] M. Hanfland, H. Beister, and K. Syassen, Phys. Rev. B **39**, 12 598 (1989).
[5] R.J. Nemanich, G. Lucovsky, and S.A. Solin, Solid State Commun. **23**, 117 (1977).
[6] M. Hanfland, K. Syassen, and R. Sonnenschein, Phys. Rev. B **40**, 1951 (1989).
[7] G. Bellodi, A. Borghesi, G. Guizzeti, L. Nosenzo, E. Reguzzoni, and G. Sammoggia, Phys. Rev. B **12**, 5951 (1975).
[8] R. Nicklow, N. Wakabayasi, and H.G. Smith, Phys. Rev. B **15**, 4951 (1977).
[9] O.L. Blakslee, D.G. Proctor, E.J. Seldin, G.B. Spence, and T. Wing, J. Appl. Phys. **41**, 3373 (1970); E. Seldin and C.W. Nezbeda, *ibid.* **41**, 3389 (1970).
[10] P.M. Williams, Nuovo Cimento **38B**, 216 (1977).
[11] W. Eberhardt, I.T. McGovern, E.W. Plummer, and J.E. Fisher, Phys. Rev. Lett. **21**, 200 (1980).
[12] A.R. Law, J.J. Bary, and H.P. Hughes, Phys. Rev. B **28**, 5332 (1983).
[13] T. Takahashi, H. Tokailin, and T. Sagawa, Phys. Rev. B **32**, 8317 (1985).
[14] V. Dose, G. Reusing, and H. Scheidt, Phys. Rev. B **26**, 984 (1982).
[15] D. Marchand, C. Frétigny, M. Laguës, F. Batallain, Ch. Simon, I. Rosenman, and R. Pinchaux, Phys. Rev. B **30**, 4788 (1984).
[16] R. Claessen, H. Cartensen, and M. Skibowski, Phys. Rev. B **38**, 12 582 (1988).
[17] I.R. Collins, P.T. Andrews, and A.R. Law, Phys. Rev. B **38**, 13 348 (1988).

[18] F. Maeda, T. Takahashi, H. Ohsawa, S. Suzuki, and H. Suematsu, Phys. Rev. B **37**, 4482 (1988).
[19] J.W. McClure, Phys. Rev. **108**, 612 (1957).
[20] J.C. Slonczewski and P.R. Weiss, Phys. Rev. **109**, 272 (1958).
[21] M.S. Dresselhaus and G. Dresselhaus, Phys. Rev. B **13**, 4635 (1976).
[22] For a recent review, see R. Clark and C. Uher, Adv. Phys. **33**, 469 (1984).
[23] A. Zunger, Phys. Rev. B **17**, 626 (1978).
[24] R.C. Tatar and S. Rabii, Phys. Rev. B **25**, 4126 (1982).
[25] H.J.F. Jansen and A.J. Freeman, Phys. Rev. B **35**, 8207 (1987).
[26] D.A. Fisher, R.M. Wentzcovitch, R.G. Carr, A. Continenza, and A.J. Freeman, Phys. Rev. B **44**, 1427 (1991).
[27] N.A.W. Holzwarth, S.G. Louie, and S. Rabii, Phys. Rev. B **26**, 5382 (1982).
[28] J.-C. Charlier, X. Gonze, and J.-P. Michenaud, Phys. Rev. B **43**, 4579 (1991).
[29] M.C. Schabel and J.L. Martins, Phys. Rev. B **46**, 7185 (1992).
[30] S. Auluck and M.S.S. Brooks (unpublished).
[31] J.M. Wills (unpublished); J.M. Wills and B.R. Cooper, Phys. Rev. B **36**, 3809 (1987); D.L. Price and B.R. Cooper, *ibid.* **39**, 4945 (1989).
[32] O.K. Andersen, Phys. Rev. B **12**, 3060 (1975).
[33] H.L. Skriver, *The LMTO Method* (Springer, Berlin, 1984).
[34] D.J. Chadi and M.L. Cohen, Phys. Rev. B **8** 5747 (1973); S. Froyen, *ibid.* **39**, 3168 (1989).
[35] L. Hedin and B.I. Lundqvist, J. Phys. C **4**, 2064 (1971).
[36] C.S. Wang and W.E. Pickett, Phys. Rev. Lett. **51**, 597 (1988).
[37] J.C. Bowman and J.A. Krumhansl, J. Phys. Chem. Solids **6**, 367 (1958); P.H. Keesom and N. Pearlman, Phys. Rev. **99**, 1119 (1955).
[38] A. Bianconi, S.B.M. Hagström, and R.Z. Bachkrach, Phys. Rev. B **16**, 5543 (1977).